Article:
Sabri, M.M. and Moebus, G. (2016) Electron irradiation induced nanocrystal formation in Cu-borosilicate glass. Journal of Nanoparticle Research, 18 (3). 73. ISSN 1388-0764

https://doi.org/10.1007/s11051-016-3376-3

Electron irradiation induced nanocrystal formation in Cu-borosilicate glass

Mohammed Mohammed Sabri . Günter Möbus

Department of Materials Science and Engineering, University of Sheffield, Sheffield S1 3JD, United Kingdom

e-mail: g.moebus@sheffield.ac.uk

Abstract

Nanoscale writing of Cu-nanoparticles in glasses is introduced using transmission electron microscopy (TEM) focused irradiation. Two types of copper borosilicate glasses, one with high and one with low Cu-loading, have been tested at energies of 200 - 300 keV and formation of Cu nanoparticles in a variety of shapes and sizes using different irradiation conditions is achieved. Electron energy loss spectroscopy (EELS) analysis, combined with high resolution transmission electron microscopy (HRTEM) imaging confirmed the irradiation-induced precipitated nanoparticles as metallic, while furnace annealing of the glass triggered dendrite-shaped particles of copper oxide. Unusual patterns of nanoparticle rings and chains under focused electron beam irradiation are also presented. Conclusively, electron beam patterning of Cu-loaded glasses is a promising alternative route to well established femtosecond-laser photoreduction of Cu-ions in glass.

Keywords: Borosilicate glass . Cu nanoparticles . Electron irradiation

Introduction

Studying the effects of electron irradiation in oxide glasses is a research field with long-standing track record but also recent interest (Sun et al. 2005; Bae et al. 2007; Sun et al. 2004; Jiang and Silcox 2002; Meldrum et al. 1997; Sabri et al. 2015; Ollier et al. 2006; Möbus et al. 2008 ; Möbus et al. 2010). Electron beams induce various modifications in structure, composition and properties of the glass, such as phase separation and alkali migration (Sun et al. 2004; Jiang and Silcox 2002), precipitation (Meldrum et al. 1997; Sabri

et al. 2015), bubble formation (Ollier et al. 2006), fluidity enhancement and shape rounding (Möbus et al. 2008 ; Möbus et al. 2010).

Of particular interest is the irradiation induced generation of metal nanoparticles in glass. Nanoscale metal particles are known to exhibit physical and chemical properties, which are very different from the bulk materials (Wang et al. 2005). Copper nanoparticles together with other noble metals such as silver and gold are the most studied metallic nanoparticles. This is due to the fact that the surface plasmon resonances (SPR) feature in the optical spectra in the visible region (Yeshchenko et al. 2007). However, in comparison with Au and Ag, copper has the advantage of being low-cost and highly abundant while showing high conductivity.

Due to the high flexibility and high homogeneity of glasses they are considered to be an excellent host matrix to add different species. Copper nanoparticles embedded in silicate glasses are extremely promising materials for optical applications (Zhong et al. 2012; Teng et al. 2011) showing nonlinear optical properties (Almeida et al. 2012). The methods reported so far to precipitate copper in glass include for example ion implantation (Wang et al. 2010), femtosecond laser irradiation (Teng et al. 2010) and sol-gel followed by reduction and then nanoparticles growth via annealing (Zhong et al. 2013). Other metal nanoparticles have been generated by electron irradiation in glass as well (Jiang 2010; Singh and Karmakar 2011).

Cu in silica has been studied by Ito *et al* (Ito et al. 1999) who reported enlargement of pre-existing metallic copper nanoparticles in an amorphous SiO_2 film in scanning transmission electron microscopy. Outside the field of oxide glasses, electron beam irradiation-induced formation of copper nanoparticles of various diameters in different materials has been reported (Pham et al. 2011; Yen et al. 2004; Zhou et al. 2008).

Up to date, however, no research is known in electron irradiation-induced precipitation of Cu nanocrystals in glasses. Therefore, in the present paper we report on the *in-situ* formation of

copper nanoparticles in glass using the impact of electron beam irradiation in transmission electron microscopy with prospects of achieving high-resolution beam control and patterning capabilities in the future.

Experimental details

Glass composition and melting process

The compositions of the main oxide glasses used in this study and given acronyms of CuNBS-A and CuNBS-B across the paper are $20CuO\text{-}15Na_2O\text{-}15B_2O_3\text{-}50SiO_2$ and $1CuO\text{-}15Na_2O\text{-}15B_2O_3\text{-}69SiO_2$ (in mol.%), respectively. The motivation for the choice of the compositions is to explore a concentration range of Cu which is either as low as frequently used in laser-patterning of various Cu-silicate glasses (Almeida et al. 2012; Teng et al. 2010), or as high as to provide compatibility with some of our earlier and ongoing work on other alkali-borosilicate glasses (e.g. loaded with Zn, Ag and others, as reported elsewhere (Sabri et al. 2015; Yang et al. 2006; Yang et al. 2006)). Both Cu concentrations are low enough to fall inside the glass forming region of the underlying ternary N-B-S phase diagram. The glass batch has been prepared by mixing powders of copper oxide (CuO, purity > 99%), boric acid (H_3BO_3, purity > 99.5%), sodium carbonate (Na_2CO_3, purity ~ 99.1%) and silica sand (SiO_2, purity ~ 99.5%) to obtain 200 g glass melt. After melting in a mullite crucible and electric furnace at 1400^{o}C about 80% of the melt is poured into a pre-heated stainless steel mould while 20% is rapidly cooled by pouring into water to obtain a glass frit. The glass block was annealed at 550^{o}C with return to room temperature at 1^{o}C/min.

Sample preparation for electron microscopy

The glass frit was exclusively examined by TEM: specimens were prepared by grinding the quenched glass frit into a very fine powder in acetone using a pestle and mortar. After ultra-sonication for about 15 min the powder was placed on a holey carbon film, here supported by

a gold grid, instead of the usual copper grid, such as to avoid overlap of copper EDX signals from the glass and from the grid. The annealed glass was examined by x-ray diffraction (XRD) and both TEM and SEM. Initially the glass block is cut twice in cross section by a diamond cutting saw into a thin slice of about 2×2 cm cross section. For SEM this slice is then ground using various grit wheels and polished by a diamond paste and carbon coated against charging. For TEM and XRD, only grinding was used, making sure that the outer regions of the cross-sectional slice are cut off and excluded, as they might be less typical due to their faster cooling rate in contact with air or the metal mould.

Electron irradiation and imaging process

In this research, TEMs of type JEOL JEM 2010F field emission gun (FEG) and JEOL JEM 3010 LaB_6 thermal filament operating at 200 and 300 keV respectively have been used for the purpose of both imaging (low intensity) and deliberate electron beam (high intensity) irradiation. Electron energy loss spectroscopy (EELS) and energy dispersive x-ray (EDX) spectroscopy are used on the JEOL JEM 2010F. On both TEMs, most of the irradiation is applied with largest condenser aperture (CA) and spot size 1. Irradiation densities range from 0.01 pA/ nm^2 for low-intensity imaging over <1 pA nm^2 for our chosen "standard" converged irradiation conditions and >3 pA/ nm^2 for special high-current conditions with condenser aperture removed. On the other hand, SEM images (both secondary electron (SE) and backscattered electron (BSE)) were taken using FEI Inspect F, selected at 20 kV, also equipped with EDX.

Results

TEM irradiation and imaging of quenched glass

Three rod shaped frit CuNBS-A glass fragments were selected for different electron irradiation conditions (Fig. 1). The top row is meant to study dose variation via changes of beam current, while the bottom row contains dose variation via exposure at constant current.

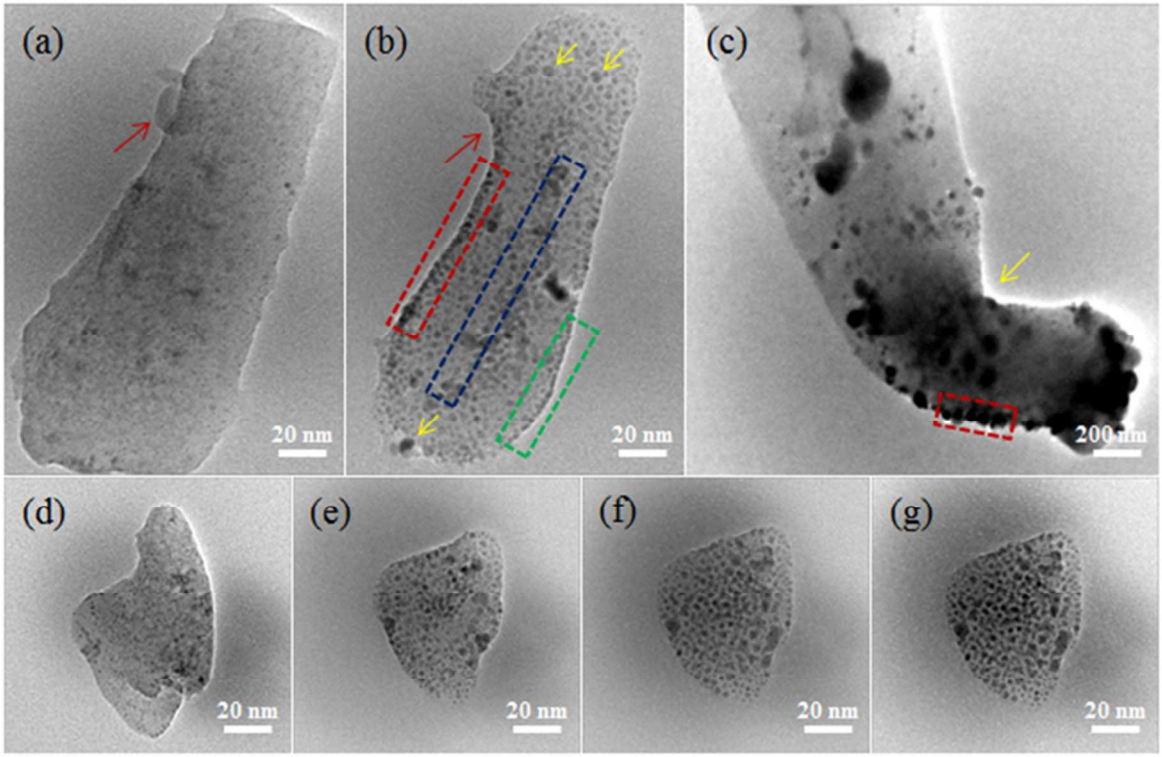

Fig. 1 TEM micrographs of frit CuNBS-A glass fragments; JEM TEM 3010 at 300 keV. (a-c): Intensity series; (a) imaging radiation only; (b) after about 3 min of standard converged electron beam irradiation. (c) similar glass fragment after irradiation with open-aperture (high current) for about 2 min. (d-g) Time series at constant intensity (standard converged beam, aperture inserted), including intervals of 3 minutes added irradiation between each image.

At the first stage, see Fig. 1a, using weak wide-beam (full screen) imaging illumination the initial glass fragment of roughly 60 nm × 250 nm size is rather homogeneous, except for

some speckle. Upon comparison with the surrounding amorphous carbon-film, some coherency-speckle existing for all amorphous materials in HRTEM can be observed (focus-dependent), and in addition we identify a small number of true clusters or precipitates, which are darker and sharper (<3 nm-sized). We believe these fine Cu clusters and small particles have formed during the early stages of focusing and preparing the electron beam for irradiation. Subsequently, the main precipitation experiment was triggered by systematic electron beam convergence to a diameter slightly larger than 200 nm for about 3 min irradiating the entire glass fragment. Fresh nanoparticles of isotropic morphologies precipitated through the entire glass fragment. The distribution of these nanoparticles is rather homogeneous and diameters range from about 1-12 nm (yellow arrows for largest NPs in Fig. 1b). These particles have grown by extraction of Cu from the glass, with the matrix getting brighter (more transparent) and include enlargements of any pre-existing clusters from Fig. 1a, but most of them are newly nucleated particles. As a side effect, some smoothing of rough surfaces of the glass fragment and rounding-off of the glass corners (Möbus et al. 2010) is observed, also including the merging (fusion/welding) of the main glass with an originally separate attached glass particle (red arrow on Fig. 1a,b). An overall shrinkage of the volume of the glass fragment indicating some ablation of the Na-B-Si-oxide network is found. Remarkably, formation of particle chains in the glass fragment is evident with the first chain being about 90 nm long and consisting of about 23 nanoparticles (indicated by red dashed area in Fig. 1b), while the opposite second chain (green dashed area in Fig. 1b) is shorter. Both are just inside the edge of the glass fragment along its long aspect. A third chain of nanoparticles can be seen in the centre of the glass fragment, again parallel to the long axis (blue dashed area in Fig. 1b), and this consists of a mixture of small and few large nanoparticles. Due to the large particle numbers involved in these very systematic chains, they are true 3D chains and cannot be a projection artefact (Xu et al. 2008). The 3rd stage of

the intensity-series involves irradiation of another glass rod-fragment (initially looking similar to Fig. 1a) via removing the condenser aperture, increasing currents by a factor 11. After ~ 2 min of electron irradiation, fewer and larger nanoparticles are formed with less circular shapes distributed very in-homogeneously through the glass rod. This indicates a growth and ripening stage, merging multiple particles, with no more Cu extracted from the glass. The residual glass matrix in regions of >200 nm is now very bright and transparent, virtually Cu-free and speckle-free. Several small nanoparticles are also stacked outside the glass rod touching its edges and some others of diameter of about 50 nm are found in an ordered state outside the glass rod, near the edge, denoted by the red dashed area in Fig. 1c. The glass rod bending (yellow arrow) of the originally straight rod is another irradiation result.

Complementary, the exposure-time series at constant current (Fig. 1d-g) reveals formation of clusters and small round particles over multiple applications of 3 min additional irradiation. This series started with pre-irradiation levels triggering cluster formation already in Fig. 1d, however, after switching to the higher current for Fig. 1e, the small particles of Fig. 1d are not traceable to grow, but rather replaced by mostly new and larger particles. This coincides with a fragment-change morphing the glass into a more roundish shape. However, the precipitation saturates quickly in Fig. 1f,g and no ripening occurs unlike in Fig 1c, indicating lack of long-range diffusion, and therefore lack of temperature.

To reveal further aspects about radiation induced precipitation mechanisms, we now switch from homogeneous illumination of an entire glass fragment to local electron beam irradiation, with beam diameter much smaller than the fragment. In such situations, beam-induced ring formation has been previously reported in silicate glasses (Jiang et al. 2003) but not so far involving copper. Figure 2a,b shows the impact of irradiation in a FEG-TEM, with beam

focused to 100-150 nm, showing the formation of nanoring-like structures of nanoparticles in the frit CuNBS-A glass.

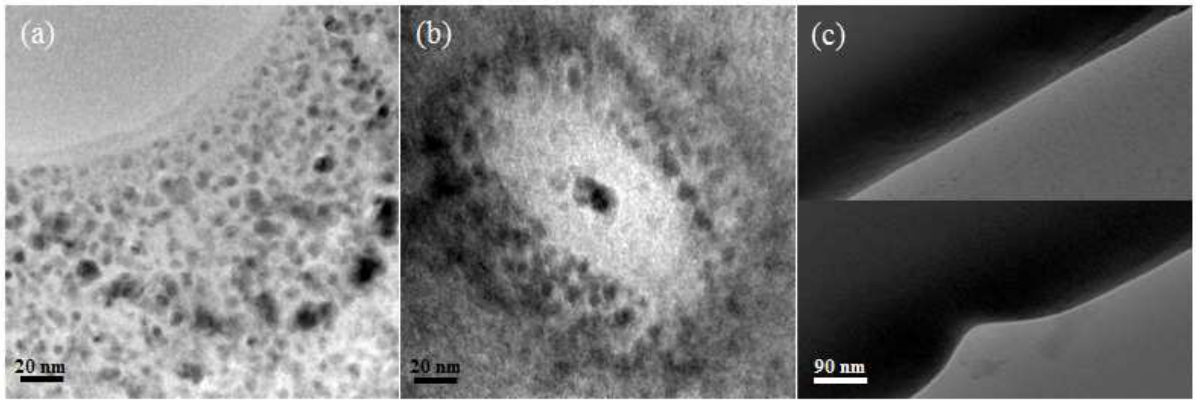

Fig. 2. (a,b) Formation of ring-like Cu nanoparticles in the glass fragment of frit CuNBS-A using focused electron beam in JEM TEM 2010F at 200 keV. (c) CuNBS-B glass before (upper) and after (lower) 6 min of electron irradiation in JEM TEM 3010 at 300 keV.

In Fig. 2a, a medium intense electron beam of diameter of about 140 nm for about 5 min irradiation generated nanoparticles of 8-15 nm size along the ring and smaller sub-10 nm NPs inside the ring. Nearby irradiation with more focused electron beam in a thicker glass fragment area (Fig. 2b) generated a dark ring with one central dark particle separated by significantly lighter areas due to Cu-depletion and/or glass matrix ablation. To compare the response of high and low Cu loaded glasses (CuNBS-A versus CuNBS-B), Figure 2c shows a glass rod of CuNBS-B being irradiated on its edge for about 6 min. No Cu nanoparticles or clusters are visible at the region under irradiation, while significant glass ablation is obvious. An EELS spectrum from the region of irradiation of glass CuNBS-A in Fig. 2a is shown in Fig. 3a.

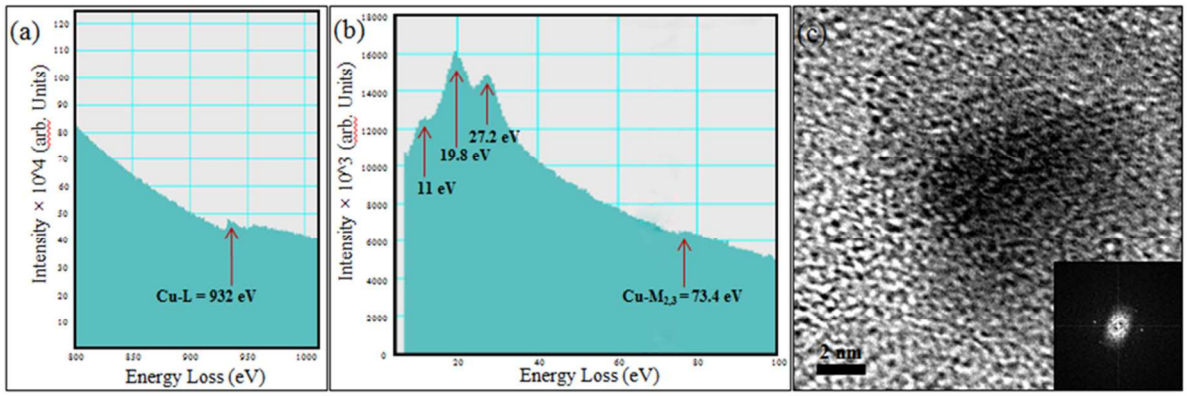

Fig. 3. EELS spectra of frit CuNBS-A glass fragments after irradiation showing (a) L-edge for particle in glass, (b) low loss spectrum showing plasmon-range peaks and $M_{2,3}$ edge for metal particle, (c) HRTEM image for a typical nanoparticle in glass with FFT as inset.

The main peak appearing in the EEL spectrum at around 932 eV with an onset around 929 eV (Fig. 3a) becomes very distinct after few minutes of irradiation, corresponding to the Cu-L edge (within expected calibration uncertainties), due to the glass matrix thinning while Cu segregation pushing Cu-concentration locally. Comparing literature data for fine structure between Cu, CuO and Cu_2O (Ito et al. 1999; Long and Petford-Long 1986; Yang et al. 2014), the shape of the L-edge of Fig. 3a clearly matches metallic copper, as oxides would show two high-contrast "white lines". Complementary, Fig. 3b shows a low loss EEL spectrum acquired on one particle as of Fig. 4e, and the peak with onset around 73.4 eV matches the $M_{2,3}$ edge, although not distinctive between metal and oxides (Ahn et al. 1983). However, two distinguishing peaks at around 19.8 and 27.2 eV respectively well match metallic copper (Ahn et al. 1983), as oxide would show a single broad peak around 22 eV. Together with the small peak at around 11 eV all those three peaks match literature data (computer modelling and earlier experiments) for metallic copper, while the origin of these "plasmon-range" peaks has been attributed to d-band interband transitions in (Hébert et al. 2011).

For further confirmation, Fig. 3c shows HRTEM of a typical precipitate NP from the irradiation region in Fig. 2a with fast Fourier transformation (FFT) as inset, from which a d-spacing can be extracted compatible with metallic copper.

It is worthwhile to expand our observations to cases where segregated and expelled Cu does not precipitate inside the glass only but deposits on the glass fragment surface or even in its vicinity of the support film as shown in Fig. 4.

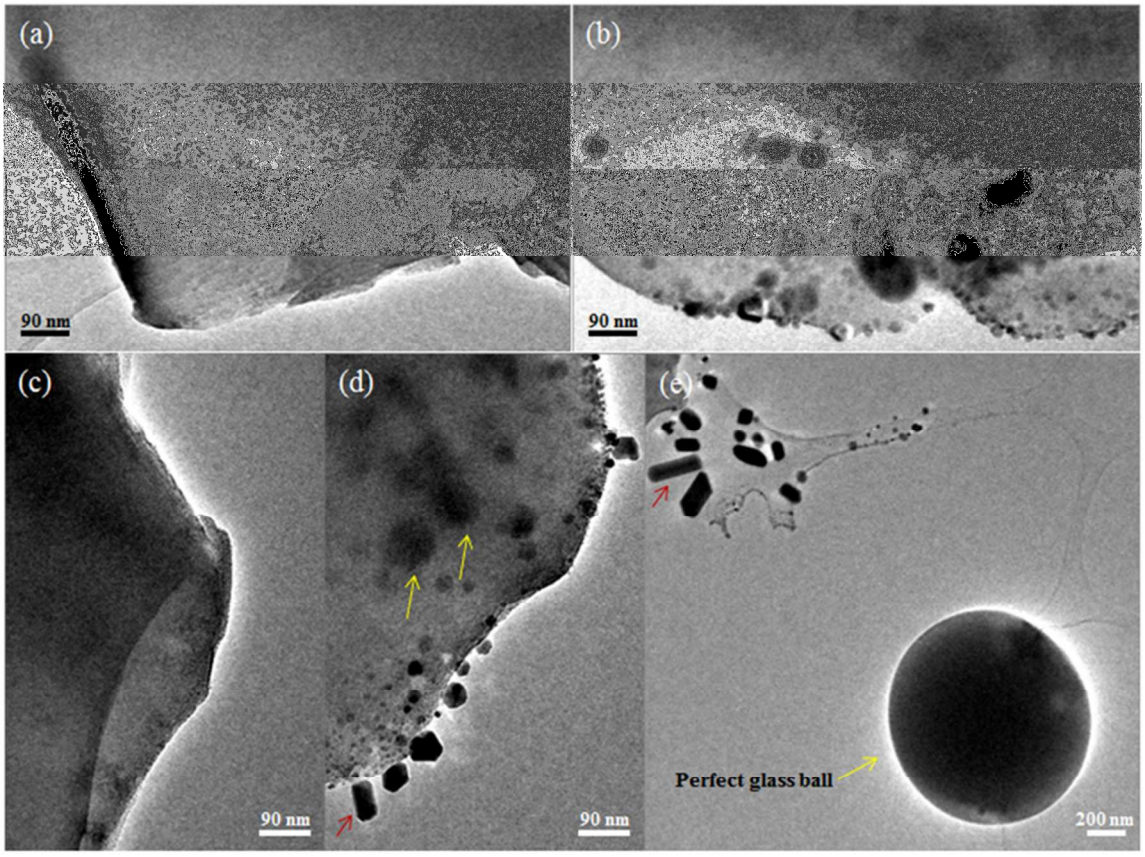

Fig. 4. Surface decoration with Cu using frit CuNBS-A glass; JEM TEM 3010 at 300 keV. (a) completely cluster and particle-free pristine glass; (b) after 2 min irradiation; (c-e): 2nd glass fragment series consists of (c) zero and (d) 2 min standard irradiation, while (e) shows delocalised formation of Cu nanocrystals on nearby C-film and sudden transformation of a glass fragment into a perfect glass ball under open-aperture high level of irradiation.

The initial views of the two glass fragments (Fig. 4a,c) are important examples where pre-irradiation was successfully minimised, such that no clusters or particles are visible at all. The speckle in the fragment is of same level than in the neighbouring carbon film, and therefore confirms coherency-speckle typical for amorphous materials while no sharp and black particles, indicating Cu, are visible. Irradiation experiments in Fig. 4b (condenser aperture inserted) and Fig. 4d (no condenser aperture), resulted in the formation of surface-deposited NPs, clearly outside the original glass perimeter. Particularly well-faceted morphology and shapes, typical of single crystal of metallic Cu, are seen in Fig. 4d. Contrary, roundish-shape NPs are still formed inside the original glass with diameter of about 5-35 nm, except for two large NPs of ~ 77 nm (yellow arrows in Fig. 4d). A large surface crystal is marked by red arrow. Another irradiation of a nearby glass fragment with condenser aperture removed resulted in formation of large-distance evaporated well-faceted Cu nanocrystals of which the largest has dimensions of about 260 nm × 64 nm (red arrow in Fig. 4e), sitting > 1 μm away from the original glass fragment which itself became transformed into a perfect ball (Möbus et al. 2010) of diameter of ~ 1 μm (Fig. 4e). We believe that the sequence of these phenomena is, (i) firstly electron irradiation-induced precipitation of metallic Cu, (ii) followed by electron beam ablation of both Cu and glass matrix with re-deposition of metallic copper onto the carbon film away from the original glass fragment, (iii) and finally transformation of the residual not yet ablated glass fragment into a perfect ball due to surface tension.

TEM and SEM imaging of annealed CuNBS-A glass

The annealed version of CuNBS-A glass has been investigated in Fig. 5.

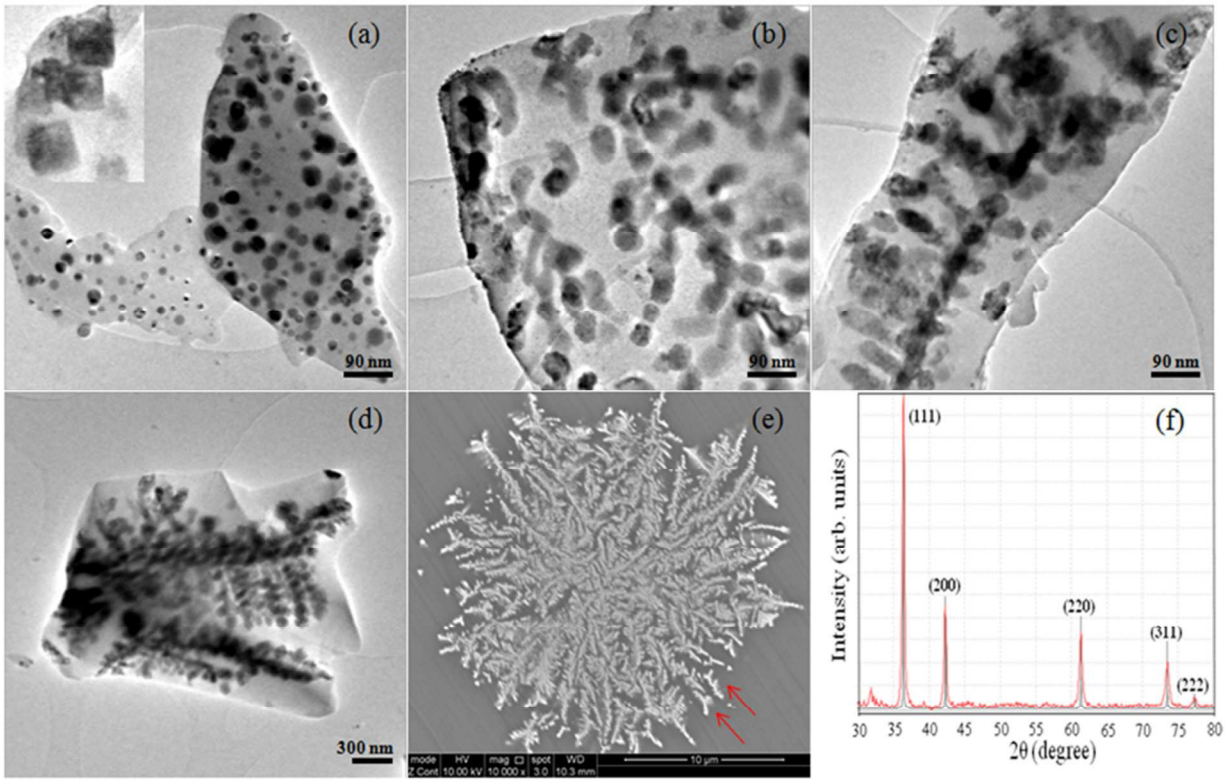

Fig. 5. (a-d) TEM (JEM TEM 3010 at 300 keV) images of annealed CuNBS-A glass spherical (a), square (the inset in (a)) and dendritic (b-d) shape of Cu_2O precipitates. (e) SEM image of a typical dendrite copper oxide particle. (f) XRD pattern of annealed CuNBS-A glass.

The precipitated nano/micro-particles, of dendrite-like shapes, are sorted by the degree of completeness of dendrite development from Figs. 5a towards 5e. The existence of various shapes, starting from spherical (Fig. 5a) and square (Fig. 5a, inset) particles up to well-developed dendrite branching systems, is due to different thermal history and temperature gradient. While we avoided inclusion of surface-near material by cutting it off, the remaining inner glass would still have experienced a cooling speed gradient as a radial function from the centre distance. The TEM images are believed to be fragments of larger dendrites, seen on

the microscale via SEM imaging (Fig. 5e). An XRD pattern of CuNBS-A glass is shown in Fig. 5f. Dominant peaks at $2\theta = 36.4^{o}$ (d=2.466 Å), $2\theta = 42.3^{o}$ (d=2.135 Å), $2\theta = 61.34^{o}$ (d=1.510 Å) and $2\theta = 73.5^{o}$ (d=1.287 Å) correspond to the planes of (111), (200), (220) and (311) of the cubic Cu_2O phase, respectively, along with a relatively weak peak at $2\theta = 77.3^{o}$ (d=1.233 Å) corresponding to (222). SEM-EDX analysis (not shown here) reveals copper oxide signals overlapping the glass matrix, while also a small Al peak shows, which is believed to be a residue from the crucible used in glass melting. The overall length of the dendrite is about 20 μm with few μm long sub-branches indicated by red arrows. The dendrites with central backbone and multi-branch structures (Fig. 5b & 5c) are consistent with Kumaran *et al* (Kumaran et al. 2013). The fact that in Fig. 5c,d the dendrite is preserved in the centre of the fragment with its backbone oriented parallel to the fracture surface during grinding indicates mechanical toughening of the glass composite material by the Cu-dendrites.

Discussions

The formation of Cu particles through electron beam irradiation seems to follow an intensity-dose dependent schedule: (i) initially very fine particles are nucleated at widely dispersed locations, sometimes even at the low intensity imaging irradiation (Fig. 1a, 1d), but this premature precipitation could be suppressed in the examples of Fig. 4a and 4c. (ii) Irradiation under standard converged beam conditions subsequently leads to further nucleation and growth of particles up to 10 nm-size range, achieved homogeneously filling the entire glass volume, with the glass matrix getting paler indicating that Cu still segregates from glass, not from other clusters. This stage is the saturated end-stage for middle intensity levels and increasing dose via time does not alter the structure, as obviously the diffusion constants for long-range diffusion necessary for Ostwald ripening are too low. (iii) Only at

extreme intensities, with open apertures, large Cu-particles grow by ripening on the cost of smaller ones, leaving Cu-free space in between, with the large diffusion distances covered by Cu atoms pointing to beam-induced heating in addition to radiation-induced fluidity (RIF).

As for surface decoration, Fig. 4, we propose that the facetted metallic Cu, surface-bound or found on the C-film, is a secondary synthesis effect upon irradiation of metallic Cu initially formed at (but still within) the glass surface, as reported for Ag in (Li and Zhang 2010) and for Co and Ni in halides in (Gnanavel and Möbus 2012). The fact that those particles form on opposite ends of C-film holes favours a kind of "thermal evaporation" deposition, rather than an atomic diffusion on the C-film itself. For the low-Cu glass (CuNBS-B) irradiation had not triggered any visible precipitation even at levels of intensity high enough to ablate the entire glass matrix. Possibly, combination of irradiation and heat treatment (which would require a TEM heating holder) would have achieved particle formation, similarly to laser induced nucleation with subsequent heat treatment (Almeida et al. 2012) for particles. Apart from observing ring formations, also centre positions in impact craters (Fig. 2b) or centre positions in rods (Fig. 1b) seem to be areas of stationary Cu location as any (e.g. electrostatic) driving force there to move these cations to the edge of glass fragment or to the edge of the beam impact area would cancel.

The purpose for including our comparative study of annealed glass fragments is to elucidate the need for suppression of thermal precipitation, confirming that a cooling-rate at least as fast as in our frit-quenching is mandatory. Indeed, further beam irradiation of the fragments in Fig. 5 did not lead to any new particles or changes to existing dendrites. The reasons why thermal annealing produces Cu_2O while "electron beam annealing" produces metallic Cu, is due to the redox environment, as we used air-furnace heating for annealing, while the TEM-exposure is a reducing medium.

Conclusions

We have demonstrated that nm-controllable electron beams can be used, complementary to the well-established laser irradiation researches, to precipitate nm-sized Cu-particles from a glass-matrix. This will be of interest for application areas ranging from glass-index grading, reflectivity engineering and wave-guiding, over surface-plasmon coupling of light or other nanoplasmonics, onto information storage and radiation-recording strategies, or most widely the modulation and modification of glass-surface appearance for visual or mechanical property tuning. Our method of open condenser aperture irradiation in TEM allowed *in-situ* observation of processes otherwise only known from thermal annealing, or from high-power electron beam instruments (e.g. welders or EPMA). Forthcoming work will extend our above results into systematic pattern generation via nm-localised automatic beam positioning and movement control.

Acknowledgments

We thank the Iraqi Kurdistan Regional Government/Ministry of Higher Education and Scientific Research for the funding of the project as a part of Human Capacity Development Program (HCDP). The authors also thank Professor Russell J Hand for his helpful contribution.

References

Ahn CC, Krivanek OL, Burgner RP, Disko MM, Swann PR (1983) Electron energy loss spectroscopy Atlas. ASU HREM Facility and Gatan, Inc

Almeida JMP, De Boni L, Avansi W, Ribeiro C, Longo E, Hernandes AC, Mendonca CR (2012) Generation of copper nanoparticles induced by fs-laser irradiation in borosilicate glass. Opt. Exp 20:15106-15113

Bae IT, Zhang Y, Weber WJ, Higuchi M, Giannuzzi LA (2007) Electron-beam induced recrystallization in amorphous apatite. Appl. Phys. Lett 90:021912

Gnanavel T, Möbus G (2012) In situ synthesis of cobalt nanocrystal hierarchies in a transmission electron microscope. J. Nanopart. Res 14:683-694

Hébert C, Alkauskas A, Löffler S, Jouffrey B, Schattschneider P (2011) Capturing EELS in the reciprocal space. Eur. Phys. J. Appl. Phys 54:33510

Ito Y, Jain H, Williams DB (1999) Electron-beam induced growth of Cu nanoparticles in silica glass matrix. Appl. Phys. Lett 75:3793-3795

Jiang N (2010) Electron-beam fabrication of nanostructures in glasses Microsc. Microsnal 16:1660-1661

Jiang N, Hembree GG, Spence JCH, Qiu J, Garcia de Abajo FJ, Silcox J (2003) Nanoring formation by direct-write inorganic electron-beam lithography. Appl. Phys. Lett 83:551-553

Jiang N, Silcox J (2002) Electron irradiation induced phase decomposition in alkaline earth multi-component oxide glass. J. Appl. Phys 92:2310-2316

Kumaran CKS, Agilan S, Velauthapillai D, Muthukumarasamy N, Thambidurai M, Balasundaraprabhu R, Senthil TS (2013) Preparation and characterization of copper dendrite like structure by chemical method. Adv. Mater. Res 678:27-31

Li K, Zhang FS (2010) Novel approach for preparing silver nanoparticles under electron beam irradiation. J. Nanopart. Res 12:1423-1428

Long NJ, Petford-Long AK (1986) In-situ electron-beam-induced reduction of CuO: A study of phase transformations in cupric oxide. Ultramicroscopy 20:151-159

Meldrum A, Boatner LA, Ewing RC (1997) Electron-irradiation-induced nucleation and growth in amorphous $LaPO_4$, $ScPO_4$, and zircon. J. Mater. Res 12:1816-1827

Möbus G, Ojovan M, Cook S, Tsai J, Yang G (2010) Nano-scale quasi-melting of alkali-borosilicate glasses under electron irradiation. J. Nucl. Mater. 396:264-271

Möbus G, Tsai J, Xu XJ, Bingham P, Yang G (2008) Nanobead formation and nanopatterning in glasses. Microsc. Microanal 14:434-435

Ollier N, Rizza G, Boizot B, Petite G (2006) Effects of temperature and flux on oxygen bubble formation in Li borosilicate glass under electron beam irradiation J. Appl. Phys. 99:073511

Pham LQ, Sohn JH, Park JH, Kang HS, Lee BC, Kang YS (2011) Comparative study on the preparation of conductive copper pastes with copper nanoparticles prepared by electron beam irradiation and chemical reduction. Radia. Phys. Chem 80:638-642

Sabri MM, Hand RJ, Möbus G (2015) Zn nanodot patterning in borosilicate glasses by electron irradiation. J. Mater. Res 30:1914-1924

Singh SP, Karmakar B (2011) In situ electron beam irradiated rapid growth of bismuth nanoparticles in bismuth-based glass dielectric at room temperature. J. Nanopart Res 13:3599-3606

Sun K, Wang LM, Ewing RC, Weber WJ (2004) Electron irradiation induced phase separation in a sodium borosilicate glass. Nucl. Instrum. Methods Phys. Res. Sect. B 218:368-374

Sun K, Wang LM, Ewing RC, Weber WJ (2005) Effects of electron irradiation in nuclear waste glasses. Philos. Mag 85:597-608

Teng Y, Qian B, Jiang N, Liu Y, Luo F, Ye S, Zhou J, Zhu B, Zeng H, Qiu J (2010) Light and heat driven precipitation of copper nanoparticles inside Cu^{2+}-doped borate glasses. Chem. Phys. Lett 485:91-94

Teng Y, Zhou J, Luo F, Lin G, Qiu J (2011) Controllable space selective precipitation of copper nanoparticles in borosilicate glasses using ultrafast laser irradiation. J. Non-Cryst. Solids 357:2380-2383

Wang X, Zhuang J, Peng Q, Li Y (2005) A general strategy for nanocrystal synthesis. Nature 431:121-124

Wang YH, Wang YM, Lu JD, Ji LL, Zang RG, Wang RW (2010) Nonlinear optical properties of Cu nanoclusters by ion implantation in silicate glass. Opt. Commu 283:486-489

Xu X, Saghi Z, Yang G, Hand RJ, Möbus G (2008) Three-dimensional structure of CeO_2 Nanodendrites in Glass. Cryst. Growth Des 8:1102-1105

Yang G, Cheng S, Li C, Zhong J, Ma C, Wang Z, Xiang W (2014) Investigation of the oxidation states of Cu additive in colored borosilicate glasses by electron energy loss spectroscopy. J. Appl. Phys 116:223707

Yang G, Möbus G, Hand RJ (2006) Cerium and Boron Chemistry in Doped Borosilicate Glasses Examined by EELS. Micron 37:433-441

Yang G, Möbus G, Hand RJ (2006) EELS Study of Boron Coordination in Alkali Borosilicate Glasses under Extensive Electron Irradiation. Phys. Chem. Glass 47:507-512

Yen MY, Chiu CW, Chen FR, Kai JJ, Lee CY, Chiu HT (2004) Convergent electron beam induced growth of copper nanostructures: Evidence of the importance of soft template. Langmuir 20:279-281

Yeshchenko OA, Dmitruk IM, Dmytruk AM, Alexeenko AA (2007) Influence of annealing conditions on size and optical properties of copper nanoparticles embedded in silica matrix. Mater. Sci. Eng 137:247-254

Zhong J, Xiang W, Chen Z, Zhao H, Liang X (2013) Structural, Linear and third-order nonlinear optical properties of Cu nanocrystal in sodium borosilicate glass. Mater. Sci. Eng. B 178:998-1003

Zhong J, Xiang W, Zhao H, Zhao W, Chen G, Liang X (2012) Synthesis, characterization, and third-order nonlinear optical properties of copper quantum dots embedded in sodium borosilicate glass. J. Alloys. Compd 537:269-274

Zhou R, Wu X, Hao X, Zhou F, Li H, Rao W (2008) Influences of surfactants on the preparation of copper nanoparticles by electron beam irradiation. Nucl. Instrum. Methods Phys. Res. Sect. B 266:599-603